CLIMATOLOGY

Protected areas provide thermal buffer against climate change

Xiyan Xu[1]*, Anqi Huang[2], Elise Belle[3], Pieter De Frenne[4], Gensuo Jia[1]*

Climate change is pushing temperatures beyond the thermal tolerance of many species. Whether protected areas (PAs) can serve as climate change refugia for biodiversity has not yet been explored. We find that PAs of natural (seminatural) vegetation effectively cool the land surface temperature, particularly the daily maximum temperature in the tropics, and reduce diurnal and seasonal temperature ranges in boreal and temperate regions, as compared to nonprotected areas that are often disturbed or converted to various land uses. Moreover, protected forests slow the rate of warming more at higher latitudes. The warming rate in protected boreal forests is up to 20% lower than in their surroundings, which is particularly important for species in the boreal where warming is more pronounced. The fact that nonprotected areas with the same type of vegetation as PAs show reduced warming buffer capacity highlights the importance of conservation to stabilize the local climate and safeguard biodiversity.

INTRODUCTION

Protected areas (PAs) have long been used for conserving biodiversity and maintaining ecosystem services. They can provide relatively undisturbed habitats to protect threatened and endangered species. Land conservation practices around PAs have shown to effectively reduce deforestation (*1*) and buffer rapid agricultural and urban expansion (*2*). Without legal protection, natural vegetation in non-protected areas (NPAs) is often disturbed or converted to various forms of land use, which constitutes the major threat to biodiversity (*3*). Land disturbance and conversion not only result in habitat and biodiversity loss but also affect Earth's climate (*4*, *5*) and increase the occurrence of climate extremes (*6*). Climate change and increased occurrences of climate extremes, particularly hot episodes, are pushing a growing number of animal and plant species toward local extinction when temperatures exceed their thermal tolerance limits (*7*, *8*).

PAs play a key role in the sequestration and storage of carbon from the atmosphere into ecosystems and provide refuges for threatened species and are recognized as nature-based solutions to climate change adaption and mitigation (*9*–*11*). The aim of nature climate solutions to stabilize climate warming at the global scale is to make use of the characteristics of healthy ecosystems to increase carbon storage and cut greenhouse gas emissions while also enhancing biodiversity (*12*, *13*). Globally, more than 16% of the land area is currently protected, and this stores between 12 and 16% of land carbon stocks (*14*, *15*). Land-use change in these PAs, especially in forests, can have substantial effects on the global mean temperature, not only via enhanced greenhouse effects but also via nonlocal biogeophysical climate feedbacks. These nonlocal effects on global mean temperature can be substantial (*16*, *17*).

However, biodiversity and its response to climate change are largely determined by microclimate that is modulated by local habitats and landscape features at the local scale (*18*–*20*). The modified landscapes have complex impacts on the local land surface and air temperatures through altered evapotranspiration (ET), surface albedo, and aerodynamic resistances (*21*–*23*). Land conversion from natural vegetation to croplands, which has been shown to have a net warming effect in the tropics, may have a neutral or net cooling effect in northern latitudes (*24*). However, the potential of PAs to maintain microclimate at local scales and buffer habitats from anthropogenic climate change has, so far, not been explored globally.

Here, we quantify the effects of terrestrial PAs on thermal habitats at the local scale across five major biomes, i.e., boreal (evergreen needleleaf), temperate (deciduous broadleaf), and tropical (evergreen broadleaf) forests; grasslands; and savannas. According to the 2018 World Database on Protected Areas (WDPA) (*25*) and Moderate Resolution Imaging Spectroradiometer (MODIS) land cover classification of 2018 (*26*), these five biomes account for about 63% of the global PA network and 79% of the terrestrial PAs with natural or seminatural vegetation (Fig. 1A and table S1). Species richness and abundances are often much higher inside PAs than that outside for many species (*27*), although the effectiveness of management in PAs can be compromised by external pressures and inadequate government support in some regions (*10*). Biological communities within PAs are assumed to be sustainably managed toward long-term conservation aims, and their conditions are considered to be optimal under the current climate state. NPAs of the same natural or seminatural vegetation and climate as nearby PAs are expected to experience more pressures than PAs. Our results demonstrate that PAs tend to have larger leaf area index (LAI) values than the NPAs, characterizing higher amount of foliage in the canopy that drives physiological and biophysical processes (fig. S1).

We use MODIS 8-day Aqua land surface temperature (LST) dataset (MYD11A2 version 6) (*28*) at 1-km spatial resolution to quantify the LST modulated by PAs. The overpass time of Aqua is around 1:30 p.m. and 1:30 a.m. local time, which approximates the times of daily maximum and minimum temperatures, respectively. The daily means and ranges of LST are calculated as the mean and difference of the daily maximum and minimum LST, respectively. The seasonal variations of LST are calculated as the difference of LST in local summer and local winter. Furthermore, temporal trends of the annual mean LST and air temperature are analyzed for each biome with different PA coverage to explore whether PAs can buffer the warming trend of temperatures.

[1]Key Laboratory of Regional Climate-Environment for Temperate East Asia, Institute of Atmospheric Physics, Chinese Academy of Sciences, Beijing 100029, China. [2]School of Geographical Sciences, Nanjing University of Information Science and Technology, Nanjing 210044, China. [3]WCMC Europe, 26 rue d'Edimbourg, 1050 Bruxelles, Belgium. [4]Forest & Nature Lab, Department of Environment, Ghent University, Gontrode-Melle, Belgium.
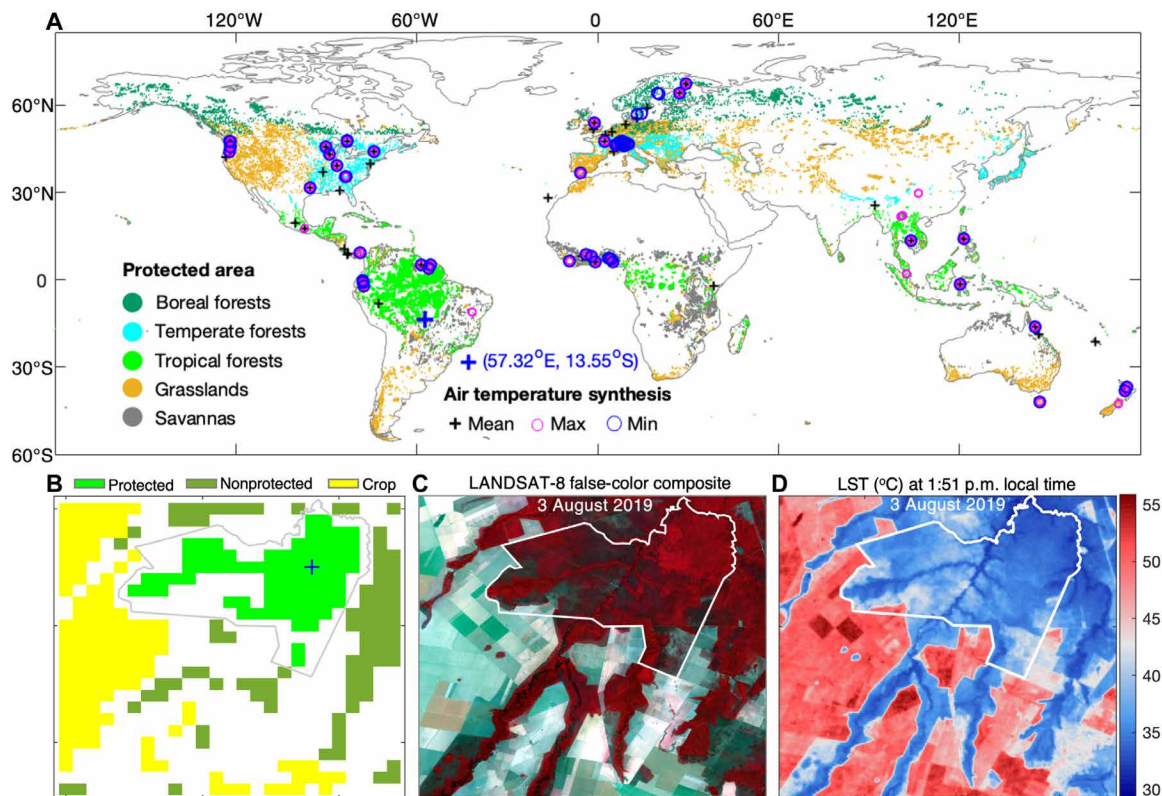*Corresponding author. Email: xiyan.xu@tea.ac.cn (X.X.); jiong@tea.ac.cn (G.J.)

Fig. 1. PAs by land cover type. (**A**) WDPA, October 2018 release, classified with MODIS land cover classification as of 2018 for boreal, temperate, and tropical forests; savannas; and grasslands. (**B**) Example of land cover classification for protected tropical forests in light green, nonprotected tropical forests in dark green, and croplands in yellow, at 1-km resolution in a 0.25° window in Brazil (57.32°E, 13.55°S). (**C**) Example of LANDSAT-8 false-color composite of band 5 (near infrared), 4 (red), and 3 (green) at 30-m resolution for a 0.25° window. (**D**) Example of LANDSAT-8 instantaneous LST at 1:51 p.m. local time in a 0.25° window retrieved from band 10 (thermal infrared) at 100-m resolution. The sites where daily mean (mean), maximum (max), and minimum (min) air temperatures were measured within and outside forest canopies are shown in (A). The polygons in (B) to (D) denote PA boundaries.

RESULTS

PAs buffer thermal environment

PAs show a higher probability of cooler daily maximum and warmer daily minimum temperatures than NPAs with the same biome (fig. S2) and croplands inferring a full conversion of land cover (fig. S3). More than 95 and 60% of protected forests show lower daily maximum temperatures than croplands and NPAs, respectively. Daily maximum LST of protected boreal, temperate, and tropical forests is 1.31° ± 0.02°C (means ± SEM), 2.24° ± 0.03°C, and 4.71° ± 0.06°C lower than that of croplands, respectively, and 0.16° ± 0.01°C, 0.57° ± 0.02°C, and 0.49° ± 0.01°C lower than that of NPAs, respectively.

PAs maintain a lower daily mean LST compared to croplands and NPAs in all biomes due to the dominant cooling effects on the daily maximum temperature (Fig. 2, A and B). Daily mean LST of protected boreal, temperate, and tropical forests is 0.22° ± 0.02°C, 0.72° ± 0.02°C, and 2.53° ± 0.03°C lower than that of croplands, respectively. The cooling contribution of protected relative to nonprotected forests to daily mean LST is less pronounced and shows larger spatial heterogeneity than that relative to croplands (Fig. 2B). This is because disturbances in NPAs tend to be lower and more heterogeneous in comparison to thorough conversion to croplands. Nevertheless, the cooling contribution of protected relative to nonprotected forests to daily mean LST follows the same latitudinal gradient as compared to land conversion, being higher in tropical

forests (ΔLST = −0.32° ± 0.01°C) than temperate forests (−0.29° ± 0.01°C) and negligible in boreal forests (−0.05° ± 0.01°C). Compared to forests, the cooling effects of protected savannas and grasslands are more spatially variable. The LST of protected grasslands is 0.32° ± 0.01°C lower than that of nonprotected grasslands and 0.19° ± 0.02°C lower than that of croplands. The LST of protected savannas is 0.29° ± 0.01°C and 1.26° ± 0.02°C lower than that of nonprotected savannas and croplands, respectively.

PAs buffer the daily range of LST because land conversion and disturbances cause asymmetric daytime maximum and nighttime minimum LST changes (Figs. 2, C and D, and 3, A and B). The mean daily ranges of LST are relatively low in forests and high in grasslands (fig. S4A). PAs show consistently lower daily ranges of LST than surrounding croplands throughout the year. This is due to the fact that the magnitude of LST changes in response to land conversion and disturbance is higher during daytime than nighttime (figs. S2 and S3). Land conversion from PAs to croplands can lead to an increased latitudinal gradient of daily ranges of LST, with the largest increase in daily range of LST being found in tropical forests (4.43° ± 0.06°C), followed by temperate forests (3.05° ± 0.03°C), savannas (2.24° ± 0.03°C), boreal forests (2.16° ± 0.03°C), and grasslands (1.26° ± 0.03°C).

The increase in daily range of LST in response to land conversion in temperate and boreal regions is due to daytime positive and

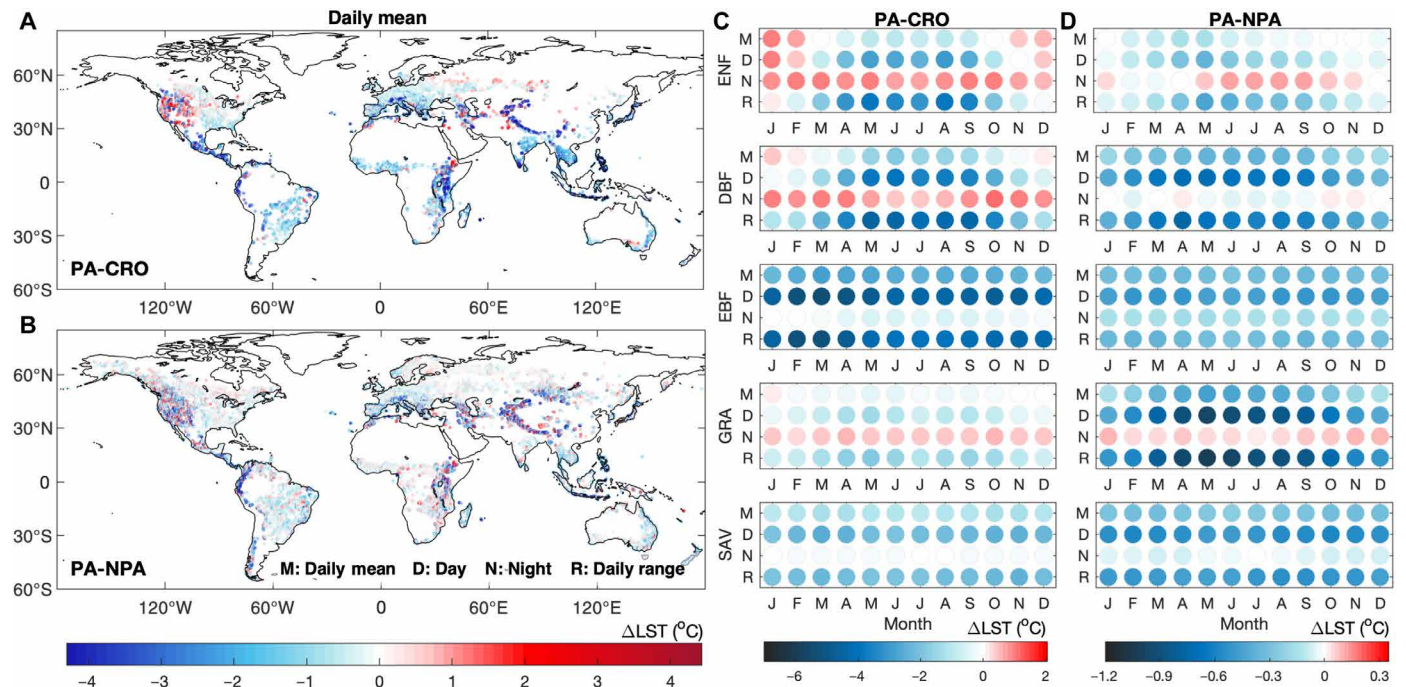**Fig. 2. Influence of PAs on LST.** (**A**) Mean LST difference between PAs and croplands ($LST_{PA} - LST_{CRO}$) and (**B**) between PAs and NPAs with the same vegetation type ($LST_{PA} - LST_{NPA}$). (**C**) Annual cycle of the daily mean (M), daytime (D), nighttime (N), and daily range (R) of LST difference between PAs and croplands and (**D**) between PAs and NPAs for boreal (ENF), temperate (DBF), and tropical (EBF) forests; grasslands (GRA); and savannas (SAV).
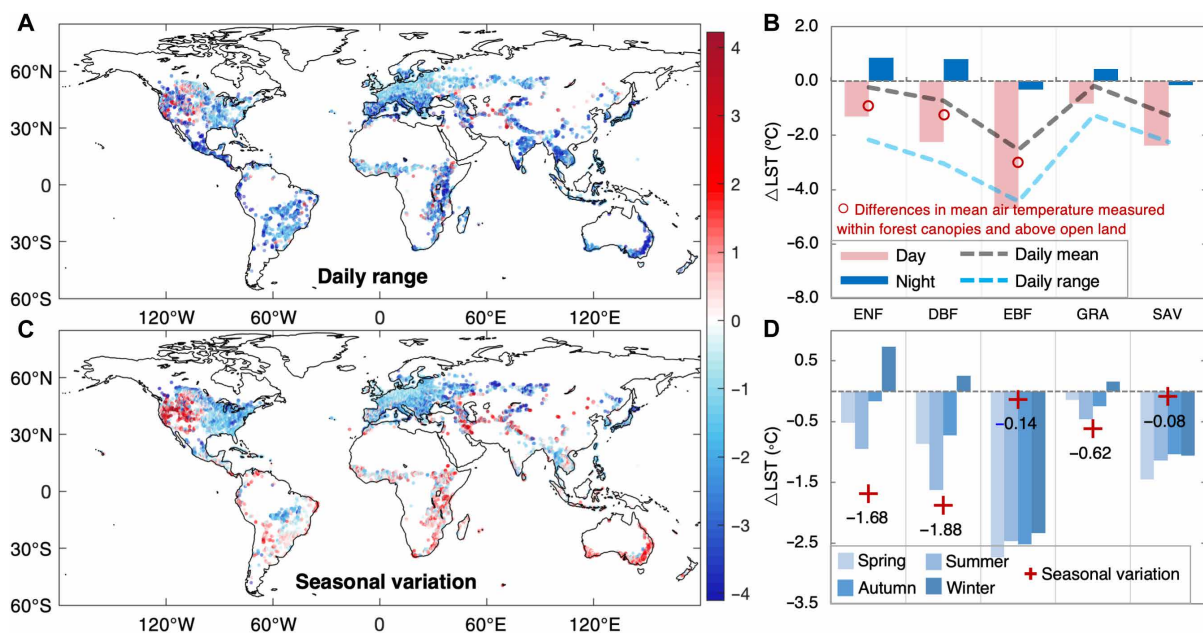

Fig. 3. Influence of PAs on daily range and seasonal variation of LST compared to croplands. (**A**) Daily range difference of LST between PAs and croplands; (**B**) daytime, nighttime, daily mean, and range of LST difference between PAs and croplands; and (**C**) seasonal variation difference of LST between PAs and croplands; and (**D**) local seasonal LST difference between PAs and croplands for boreal (ENF), temperate (DBF), and tropical (EBF) forests; grasslands (GRA); and savannas (SAV). The differences in daily mean air temperatures between the ground measurements within forest canopies and above open land for ENF, DBF, and EBF are shown in (B). The seasonal variation of LST in (C) is calculated as the LST in boreal summer (JJA) minus the LST in boreal winter (DJF). The local seasons in (D) are spring for MAM and SON, summer for JJA and DJF, autumn for JJA and DJF, and winter for DJF and JJA, for the Northern and Southern Hemispheres, respectively. The red crosses in (D) denote the seasonal variations of LST by subtracting the LST in local winter from the LST in local summer.

nighttime negative change of LST. Protected boreal and temperate forests and grasslands tend to cool the land surface during daytime and warm it during nighttime. Protected biomes show lower daily ranges of LST than nonprotected biomes on average, although the daily ranges of LST show high spatial heterogeneity (Figs. 2D and 4, A and B). Disturbances lead to the highest increase in daily range of LST in temperate forests (−0.55° ± 0.02°C) and grasslands (−0.77° ± 0.02°C). Furthermore, contrasting daily temperature ranges modified by land conversion and disturbance are higher in the warm season than in the cold season, in both temperate and boreal regions.

PAs moderate seasonal variation of thermal environment

PAs maintain a stable seasonal LST variation, while land disturbance and conversion result in asymmetric seasonal LST changes and increase the seasonal variation of LST (Fig. 3, C and D). The LST difference between the boreal summer [June to August (JJA)] and winter [December to February (DJF)] shows an opposite seasonal variation in the Northern and Southern Hemispheres, and the magnitude of seasonal LST variation increases from the tropics to high latitudes (fig. S4B). Land disturbance and conversion lead to a different LST change in the warm season (stronger warming) compared to the cold season (weaker warming or cooling) for boreal and temperate regions where the seasonal temperature variation is naturally high (Fig. 2, C and D). Protected temperate and boreal biomes cool the land surface in the local summer (JJA for the boreal summer and DJF for the austral summer) and warm the land surface in the local winter, thereby reducing the seasonal temperature variations compared to croplands. By contrast, land conversion to croplands results in increased LST variation between local summer and winter by 1.88° ± 0.02°, 1.68° ± 0.02°, and 0.62° ± 0.02°C in temperate forests, boreal forests, and grasslands, respectively (Fig. 3, C and D). PAs

also show lower seasonal variation of LST than NPAs, particularly in temperate forests (−0.14° ± 0.01°C) and grasslands (−0.37° ± 0.01°C), although the difference is less pronounced than that compared to croplands (Fig. 4, B and D).

Land conversion has relatively consistent impacts on the LST throughout the seasons in tropical forests and savannas, only leading to slightly increased seasonal LST variation between local summer and winter. This is because the seasonality of tropical and subtropical regions is characterized by the seasonal rainfall cycle exhibiting wet and dry seasons rather than contrasting cold and warm seasons. The protected tropical forests and savannas, however, show a greater cooling effect in the dry season than in the wet season. In savannas, where the wet and dry season contrast is more evident, the cooling effect of protected savannas in the dry season is about 0.16°C greater than that in the wet season.

PAs stabilize climate warming

PAs also stabilize local climate warming. The increase in annual mean LST and 2-m air temperature (Ta) between 2003 and 2018 in areas with high PA coverage is lower than in areas with low PA coverage (Fig. 5). For all biomes, the warming rates in PAs are lower than in their surrounding regions, suggesting that PAs buffer land surface warming over time. The mean warming rate in protected boreal forests is up to 20% lower than the warming rate in their surrounding regions. Meanwhile, the intensity of warming decreases with increased coverage of PAs, thereby suggesting that the buffering effect of PAs on annual mean temperature is beyond areas of conservation. This buffering effect is strongest in boreal and temperate forests where climate warming is more pronounced (Fig. 5, A and B). For each 10% increase in PA coverage, the land surface warming is slowed down by about 0.044° ± 0.008°C per decade in boreal forests,
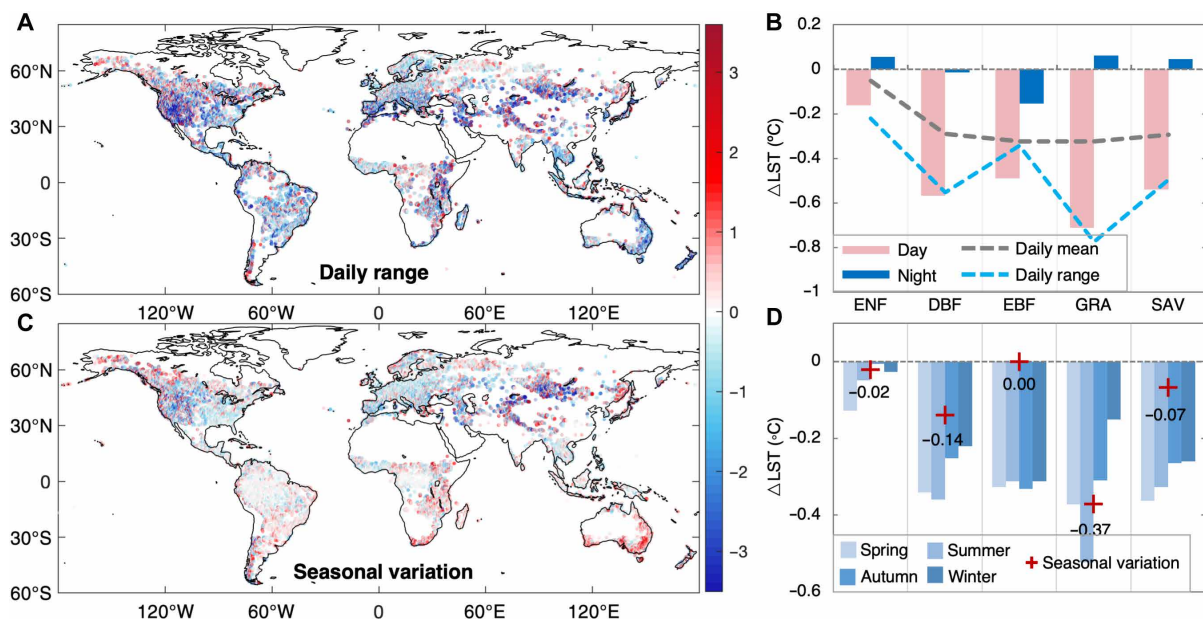

Fig. 4. Influence of PAs on daily range and seasonal variation of LST compared to NPAs. (**A**) Daily range difference of LST between PAs and NPAs; (**B**) daytime, nighttime, daily mean, and range of LST difference between PAs and NPAs for different biomes; (**C**) seasonal variation difference of LST between PAs and NPAs; and (**D**) local seasonal LST difference between PAs and NPAs for boreal (ENF), temperate (DBF), and tropical (EBF) forests; grasslands (GRA); and savannas (SAV). The seasonal variation of LST in (C) is calculated as the LST in boreal summer (JJA) minus the LST in boreal winter (DJF). The local seasons in (D) are defined as spring for MAM and SON, summer for JJA and DJF, autumn for JJA and DJF, and winter for DJF and JJA, for the Northern and Southern Hemispheres, respectively. The red crosses in (D) denote the seasonal variations of LST by subtracting the LST in local winter from the LST in local summer.

0.052° ± 0.003°C per decade in temperate forests, 0.015° ± 0.005°C per decade in tropical forests, 0.030° ± 0.009°C per decade in grasslands, and 0.0018° ± 0.005°C per decade in savannas. The slower land surface warming in areas of high PA coverage is significant across the five biomes ($P < 0.05$).

As climate change is often measured with surface air temperature, we also assessed the warming of air temperatures in relation to PA coverage. The buffering effect of PAs on air temperatures across biomes resembles that of LST, with the most notable effects in boreal (−0.041° ± 0.001°C per decade) and temperate forests (−0.018° ± 0.001°C per decade), followed by grasslands and savannas, and the lowest in tropical forests. However, the buffering effect of PAs on air temperatures is lower than that on LST. Moreover, the annual mean air temperature is much higher than the LST observed from

satellite measurements in forests (fig. S5, A to C). The buffering effects of PAs on air temperature, which are less pronounced than that on the LST, indicate the enhanced buffering effects of increased coverage of PAs on the macroclimate because air temperatures were synthesized from standard weather stations, which are mostly situated outside forest canopies (29, 30). Although the air temperatures in the reanalysis dataset with a coarse resolution are insensitive to surface processes associated with land surface heterogeneity (31), they show the buffering effects of PAs propagated to the regional scale through land-atmosphere interactions. The buffering effects on LST include the combined buffering effects of PAs on both macroclimates and microclimates because LSTs were observed from continuous satellite measurements passing above both open land and natural vegetation.
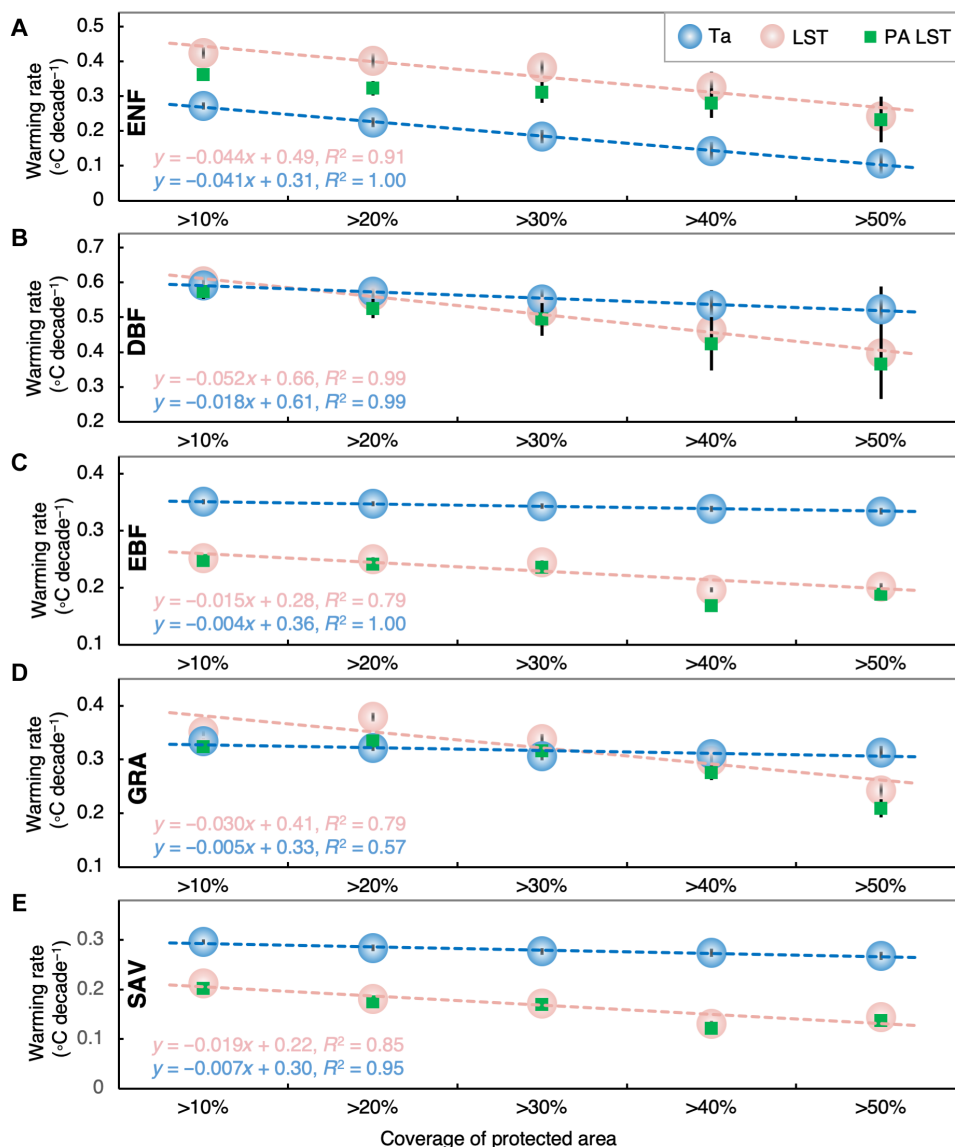

Fig. 5. Warming rates over the 2003–2018 time period according to PA coverage. Warming rate (degrees Celsius per decade) of annual mean 2-m air temperature (Ta) and LST in 0.25° gridcells and warming rate of LST in PAs only (PA LST) for (**A**) boreal (ENF), (**B**) temperate (DBF), and (**C**) tropical (EBF) forests; (**D**) grasslands (GRA); and (**E**) savannas (SAV). The warming rate is the mean slope of linear regression of annual mean Ta and LST in each 0.25° gridcell during the 2003–2018 time period. The error bars in black are the SEM warming rate for each category of PA coverage.

DISCUSSION

In this study, we use the daily maximum and minimum LST to evaluate the thermal buffering capacity of global PAs. The daily maximum LST measures the canopy temperatures in vegetated areas around noon, when shortwave radiation penetrates deep into the vegetation canopy, indicating the critical temperature-dependent physiological processes and associated energy fluxes occurring within the vegetation canopy (32). MODIS LST has been developed using the constraints of MODIS Cloud Mask data product and is thus only available under clear-sky conditions. The clear-sky LST can better represent the high and low temperature limits that determine the physiological tolerance of species (33), although it could amplify the mean temperature effects compared to all-sky conditions because clouds cool daytime and warm nighttime LSTs. The mean difference in daily mean, daytime, and nighttime LST between PAs and croplands is consistent with the daily mean, maximum, and minimum air temperature differences from 714 paired measurements within and outside forest canopies for boreal, temperate, and tropical forests (slope = 1.29, R^2 = 0.86) (figs. S6 and S7).

Protected forests can effectively cool the land surface. The latitudinal gradient of the cooling effects of protected forests on LST, i.e., decreasing cooling effects from the tropics to the poles, is similar to the spatial pattern of cooling effects of forest cover on land surface (21). This spatial pattern is also supported by ground observations of air temperatures measured within and outside forest canopies, indicating that the below-canopy microclimate is buffered by tree canopies. The buffering effect of forests on subcanopy microclimate tends to be greater than the magnitude inferred from LST that represents the temperature at the top of the canopy. Subcanopy air temperatures are even lower, most likely because of the shading and light interception of the canopy structure (20). However, the effect is much stronger than the mean effect of forests (protected and nonprotected) on LSTs compared to open land (grasslands and croplands). The cooling effects are high in tropical and temperate forests, where deforestation nevertheless results in a net warming impact on land surface and air temperature (22). Protected tropical forests and savannas, which are about 2.53° and 1.26°C cooler than nearby croplands, respectively, are key to prevent biodiversity loss because of the greater extinction risks in the tropics due to the combined effect of climate change, land-use change, and forest disturbance (34, 35).

Protected tropical forests cool the land surface more efficiently during the day than the night, which substantially reduces the daily variation of LST. Most tropical species have evolved to live within a narrow temperature range with low physiological thermal-safety margin (36) and are very sensitive to thermal range changes (37). Rising maximum temperatures due to land conversion and disturbance in particular can often lead to temperatures exceeding the thermal limits of species. A maximum temperature increase of 2.86°C is predicted to drive more than 35% of species to local extinction, even if some species can disperse and shift their climatic niches in response to the warming (7). Increase in the mean maximum temperature due to land conversion can also be catastrophic for some species. In particular, tropical species, despite having the highest thermal tolerance limits, are experiencing habitat temperatures near their thermal limits because of their nonlinear metabolic response to warming (38). Species in tropical forests are therefore likely to be more vulnerable to warming than species found in temperate and boreal forests, even if mean tropical warming rates are less pronounced. PAs in these habitats can provide key thermal refugia from episodes of extreme heat.

The thermal buffer of boreal forests is less pronounced and more variable than that of temperate and tropical forests. This could constitute a limit to the nature climate solution of afforestation and reforestation at high latitudes (39). As we have shown, the low cooling effect results from the influences of forests on temperature offset between daytime and nighttime and between summer and winter. Despite this relatively low potential to reduce mean temperatures, conservation of temperate and boreal forests tends to reduce the daily and seasonal maximum temperatures and increase the minimum temperatures, which can contribute to keeping temperatures within the critical thermal limits of temperate and boreal species. As cold tolerance limits of many ectothermic species decline with latitude (40), the buffering effect provided by PAs in temperate and boreal regions can provide important refugia for these species during nighttime and the cold season. Meanwhile, the heat tolerance limits and acclimation capacity of plant species that developed as a result of biogeographical processes are low in the mid-to-high latitudes (41). PAs can provide shaded habitats for these plant species during daytime and the warm season, thereby regulating biotic responses to macroclimate warming (19).

We have shown that NPAs with the same natural vegetation as PAs have a reduced capability of cooling land surface and of sustaining suitable diurnal and seasonal temperature ranges. This is particularly pronounced in temperate forests and grasslands, in which about 70% of the NPAs have shown reduced capability in buffering the daily maximum temperature and diurnal temperature range. Temperate biomes have long been disturbed by intensive human activities and typically exhibit a large number of small isolated patches in the populated regions of East Asia, Europe, and the United States (Fig. 4), where disturbances have altered the microclimate to a greater extent than that of other biomes (42). Habitat fragmentation also reduces the climate connectivity that normally allows organisms to shift their distributions in response to climate change (43, 44). In this context, PAs often provide the last refugia for many species threatened of local extinction in temperate forests and grasslands.

The buffering effect of PAs on increased temperatures therefore stabilizes the impacts of climate change at the global level. It is generally recognized that nature conservation contributes to global climate targets by preventing carbon emission from land-use change and by enhancing carbon removal from the atmosphere (12, 14). Here, we show that the effectiveness of PAs in stabilizing the local climate cannot be ignored. The stabilized climate in regions of high PA coverage is particularly important for providing climate change refugia and protecting species and communities from the negative impacts of climate change (45), whereas land-use change and disturbances result in greater warming that modifies habitats and threatens species. The buffering effects of PAs along a latitudinal gradient, i.e., stronger buffering at higher latitudes, are particularly important for species and communities at higher latitudes, where climate warming is more pronounced than that at lower latitudes.

The buffering effects of PAs on local microclimate are mainly achieved through the moderation of energy budgets by natural intact vegetation. Natural and seminatural vegetation, particularly forests, have much higher ET and surface roughness due to dense and tall canopies than croplands, where the land surface is cooled down by turbulent heat loss (32). By contrast, forests have lower albedo than croplands and thus absorb more shortwave radiations and warm the land surface (fig. S8A). As a result, the net effect of natural vegetation on LST is largely dependent on the trade-off between albedo and turbulent heat change due to land conversion.

The albedo and turbulent heat differences between natural vegetation and croplands vary between the day and night and among the seasons and latitudes (*21*). Croplands are often irrigated and harvested seasonally, which creates asymmetric diurnal and seasonal impacts on temperatures (*46*) and can explain the differences in daily range and seasonal variation of LST change among biomes.

We find higher LAI in PAs than NPAs, which results in lower aerodynamic resistance and enhances turbulent heat transfer from the land surface to the atmosphere, thereby cooling the land surface (*47*) in temperate forests, tropical forests, grasslands, and savannas (fig. S8B). The cooling effect of land cover with higher LAI through aerodynamic resistance plays a major role in cooling the land surface compared to other biophysical effects (*48*). In boreal regions, magnified snow-albedo feedback offsets the loss of turbulent fluxes after land conversion from forests to open land. In the winter, boreal forests have a much lower albedo than open land with snow cover, which leads to warmer surfaces than that of open land (*22*, *49*). In this study, we find very low differences in the LST and energy components between protected and nonprotected boreal forests because the LAI disturbance signal was unclear (ΔLAI = −0.018). In boreal regions, human impacts on forests are much lower compared to temporary natural disturbance, e.g., wildfire (*50*), which therefore results in minor difference between protected and nonprotected forests.

Although our results demonstrate the great values of conservation in buffering thermal environment for biodiversity, a number of potential caveats in the analysis may lead to biases. Local climates are assessed with satellite-derived LST data at 1-km spatial resolution. This resolution can well represent the heterogeneous thermal habitats at the scale of conservation area of many biological communities and ecosystems (*51*); however, the influence of potential confounding factors at finer scales (e.g., slope, aspect, and canopy morphology) on thermal habitats (*52*, *53*) is not fully considered. Furthermore, the methodology applied in this study is based on the space-for-time assumption, which is demonstrated to be useful to evaluate the thermal habitat buffered by conservation at a local scale. Because of the complex interactions between land-based climate mitigation options and global biodiversity (*54*), investigations of full climate mitigation potential including biophysical and biochemical effects of land use and management at local and regional scales are encouraged.

To conclude, PAs effectively buffer LSTs and reduce their daily range and seasonal variation compared to neighboring NPAs and croplands, where macroclimate change and disturbances threaten natural habitats and biodiversity. PAs buffer climate change by slowing down the land surface and atmospheric warming along a latitudinal gradient, which is particularly important for species and communities at higher latitudes, where climate warming is more pronounced. NPAs with the same vegetation type as PAs show reduced buffering capacity. PAs are thus key to provide species with important climate change refugia by maintaining the upper and lower thermal limits of species.

MATERIALS AND METHODS
Identification of PAs, NPAs, and croplands
The WDPA is a joint project between the United Nations Environment Programme (UNEP) and the International Union for Conservation of Nature, managed by the UNEP World Conservation Monitoring Centre. It is the most comprehensive global database of marine and terrestrial PAs. The October 2018 release of the WDPA was used in this study to identify PAs (*25*). We converted the WDPA vector data into raster at 0.01° resolution and then identified the pixels with 100% coverage of PAs as "pure pixels" of PAs. The 0.01° PAs were then overlaid with MODIS land cover classification data (MCD12Q1 version 6) of 2018 at 0.01° (*26*) to identify five major biomes, i.e., boreal forests [evergreen needleleaf forests (ENF)], temperate forests [deciduous broadleaf forests (DBF)], tropical forests [evergreen broadleaf forests (EBF)], savannas (SAV), and grasslands (GRA). The savanna classified here is the combination of woody savanna and savanna in the original MODIS International Geosphere-Biosphere Programme classification. These five biomes—i.e., ENF, DBF, EBF, GRA, and SAV—are zonal vegetation and account for about 79% of the terrestrial PAs. The five biomes were further screened with the following latitudinal limits, i.e., boreal forests within 50°N to 70°N of boreal region, temperate forest within 25°N to 50°N of temperate region, tropical forests within 25°S to 25°N of tropical region, savannas within 30°S to 15°N of tropical region, and grasslands within 30°N(S) to 55°N(S) of temperate region.

We then identified NPA and cropland (CRO) pixels completely outside PAs as pure pixels of NPA and CRO with MCD12Q1 at 0.01° resolution for the five biomes within a 0.25° window. NPAs were only identified for the same natural and seminatural biome as PAs in the same 0.25° window. To reduce systematic biases that may be caused by elevation difference in the same window, we excluded the windows in which the elevation difference between PAs and NPAs and between PAs and CRO was greater than 500 m (±500 m). The global 1-km resolution land surface digital elevation model (DEM) derived from the U.S. Geological Survey 30–arc sec SRTM30 gridded DEM data created from the NASA Shuttle Radar Topography Mission (SRTM) (*55*) was used. We assumed that the background climate for paired PAs and NPAs and paired PAs and CROs was similar in each 0.25° window with an elevation difference within 500 m. Protected biomes were assumed to be at their optimal condition under the current climate state. Nonprotected biomes, however, were assumed to be exposed to more natural and human pressures than protected biomes with the same background climate and climate variability. We calculated the 5-year (2014–2018) LAI difference between the PAs and NPAs within the same 0.25° window to evaluate the vegetation condition between PAs and NPAs with MODIS LAI dataset (MOD15A2H v006) (*56*) of 500-m spatial resolution and 8-day temporal resolution, which is resampled to 1-km spatial resolution. Croplands represented areas having experienced a full anthropogenic land conversion from natural vegetation to crops under the same background climate. Therefore, the temperature difference between PAs and NPAs and between PAs and CRO of 0.01° gridcells in the same 0.25° window either indicates the thermal difference of different land covers or is assumed to be the results of disturbance to the NPA or land conversion to CRO. It is noteworthy that the 0.01° grids used to calculate the temperatures are different for the comparison between PA and NPA and between PA and CRO because it depends on the NPA or CRO availability within a 0.25° window. Although some PAs tend to be located in remote areas where anthropogenic pressures on nature are expected to be low even without legal protection (*57*), this screening with 0.25° window restricted the comparison between PAs and NPAs (or croplands) with similar natural geographic features. The total number of 0.25° windows for PA-NPA and PA-CRO pairs is provided in table S2.

As an example, we chose to display a 0.25° window from southern Amazon to show the land cover distribution of PA, NPA, and CRO with a 0.01° MCD12Q1 gridcell according to the identification processes described above (Fig. 1B). The location of the 0.01° PA gridcell in this 0.25° window is around 57.32°E, 13.55°S. The LANDSAT-8 false-color composite of band 5 (near infrared), 4 (red), and 3 (green) of 30-m resolution for this 0.25° window on 3 August 2019 is shown in Fig. 1C, in which the dark red color denotes the coverage of natural intact vegetation, while farmland blocks and infrastructures are visible within the NPAs despite high coverage of natural or seminatural vegetation. Furthermore, we found forest fragmentation within PAs, especially near the western and southern borders (Fig. 1C), indicating disturbance of the PAs. Disturbances are indeed expected to occur when PA management is poor (10). These pixels with forest fragmentation were excluded in our analysis because they were not identified as pure pixels as defined above.

LST (of LANDSAT-8 collection-2 level-2) (58) at 1:51 p.m. local time in the 0.25° window retrieved from the LANDSAT-8 band 10 (thermal infrared sensor) of 100-m resolution on 3 August 2019 for the sample window is provided in Fig. 1D. This instantaneous LANDSAT LST corresponds to a clear-day daily maximum surface temperature for which the contrast between the different land covers is evident. The daily maximum LST measures the canopy temperatures in vegetated areas around noon, when shortwave radiations penetrate deep into the vegetation canopy, indicating the critical temperature-dependent physiological processes and associated energy fluxes occurring within the vegetation canopy (32). In the vegetated areas, especially when the canopy is dense, the LST usually corresponds to the temperature at the top of the canopy rather than at the ground surface (59). The annual mean spatial distribution of albedo and ET in 0.25° windows over the 2014–2018 time period were plotted to show the albedo and ET heterogeneity related to the land cover of PA, NPA, and CRO. The albedo was resampled to 1-km resolution with MCD43A3 version 6 dataset (60) of 500-m spatial and daily temporal resolution, and the ET was resampled to 1-km resolution with MOD16A2 version 6 dataset (61) of 500-m spatial and 8-day temporal resolution.

Influence of PAs on LST
We used MODIS Aqua LST (MYD11A2 version 6) (28) at 1-km spatial resolution to quantify the local surface temperature modulated by PAs. MYD11A2 is an 8-day average of the daily 1–km–spatial resolution LST product (MYD11A1), of which cloud-contaminated LSTs were removed by using the constraints of MODIS Cloud Mask data product. Therefore, we only used LST with "mandatory QA flags" of 0 or 1, indicating that the LST was not affected by cloud. We further excluded the LST with an average error greater than 2K according to "LST error flags" to reduce bias caused by data quality. The overpass time of Aqua is around 1:30 p.m. and 1:30 a.m. local time and approximates the times of daily maximum and minimum temperatures, respectively. We first averaged the LST from 8 days to a monthly scale and then calculated a 5-year (2014–2018) monthly mean of LST to analyze the LST difference between PAs and NPAs (or CRO). In the same 0.25° window, we evaluated the ΔLST between PAs and nearby NPAs of the same biome and between PAs and nearby croplands (CRO) as

$$\Delta LST = LST_{PA} - LST_{NPA \text{ (or CRO)}} \quad (1)$$

where LST_{PA}, LST_{NPA}, and LST_{CRO} are the 5-year monthly mean LST in the same 0.25° window for PAs, NPAs, and croplands, respectively. Negative values thus reflect cooler temperatures in PAs.

The ΔLST values at 1:30 p.m. and 1:30 a.m. local time were used to represent the daytime ΔLST (D) and nighttime ΔLST (N), respectively. The differences in daily mean LST between PAs and NPAs (or CRO), ΔLST (M), were calculated as the mean of D and N. The differences in daily range of LST between PAs and NPAs (or CRO), ΔLST (R), were calculated as the difference between D and N (D – N). We calculated the monthly and seasonal difference in ΔLST to evaluate the impact of land conversion to croplands on temperatures at the seasonal scale for boreal spring [March to May (MAM)], summer (JJA), autumn [September to November (SON)], and winter (DJF). Among the five biomes we analyzed, only grasslands and savannas are distributed in both the Southern and Northern Hemispheres. Therefore, we calculated the LST difference for these biomes between local summer and local winter to identify the influence of PAs on seasonal variation and how it is modified by disturbance and land conversion. The local summer is JJA in the Northern Hemisphere and DJF in the Southern Hemisphere, while the local winter is DJF in the Northern Hemisphere and JJA in the Southern Hemisphere. Probability frequency distributions of the daytime, nighttime, daily mean, daily range, and seasonal variation of LST differences between PAs and NPAs (or CRO) for each biome were analyzed. We also calculated the mean daytime, nighttime, daily range, and seasonal variation in LST difference between PAs and NPAs (or CRO) for each biome by averaging all 0.25° windows with the same biome, which were expressed as means ± SEM. We repeated the calculation of differences in daytime, nighttime, daily mean, daily range, and seasonal variation of LST between PAs and CRO with 0.5° searching window to evaluate the sensitivities of the results to window size. The differences in daytime, nighttime, daily mean, daily range, and seasonal variation of LST between PAs and CRO were consistent between 0.25° and 0.5° windows (regression slope = 1.01, R^2 = 1.00) (fig. S9).

Air temperatures, typically measured at standard weather stations in open lands outside forests, are often used to assess the climate change. However, the air temperatures cannot accurately represent the microclimates buffered by canopies of natural or seminatural vegetation (29). A synthesis of 308 pairs of daily mean, 198 pairs of daily maximum, and 208 pairs of daily minimum air temperatures measured within forest canopies and at neighboring ambient weather stations were used to evaluate the effects of forest canopy on air temperatures (29). The distribution of measurement sites is displayed in Fig. 1A. The measurements of the maximum, minimum, and mean air temperatures were divided into three forest biomes, i.e., boreal, temperate, and tropical forests, according to their latitude as described above (table S2). Probability frequency distributions of the daily mean, maximum, and minimum air temperature differences within and outside of forest canopies were analyzed.

Influence of PAs on land surface energy budget
The land surface energy balance is expressed as

$$(1 - \alpha)SW_{\downarrow} + LW_{\downarrow} - LW_{\uparrow} = H + LE + G \quad (2)$$

where $SW_{\downarrow}$, $LW_{\downarrow}$, $LW_{\uparrow}$ are downward shortwave radiation, downward longwave radiation, and upward longwave radiation, respectively; α is surface albedo; therefore, $(1 - \alpha)SW_{\downarrow}$ is the net shortwave radiation at land surface; H, LE, and G are the latent, sensible, and

soil heat fluxes, respectively. We neglected the ground heat flux in this study. The land surface heterogeneity has been shown to modify the surface albedo, ET, and aerodynamic resistances, among others (*21–23*). These modifications determine the difference in LST between PAs, NPAs, and croplands. Here, we compared the net shortwave radiation, net longwave radiation, latent heat, and sensible heat in Eq. 2 in PAs with that in NPAs to evaluate how disturbances modify energy budgets through biophysical processes, thereby leading to LST difference between PAs and NPAs.

The MODIS albedo dataset (MCD43A3 version 6) (*60*) was used to quantify the albedo difference between PAs and NPAs (or CRO). MCD43A3 is produced daily using 16-day Terra and Aqua MODIS data at 500-m spatial resolution. MCD43A3 provides black-sky albedo (directional hemispherical reflectance) and white-sky albedo (bihemispherical reflectance) for each of the MODIS surface reflectance bands. Actual clear-sky albedo (blue-sky albedo) is calculated as the mean of black-sky and white-sky albedo because of their small differences and high correlation (*21*). The daily albedo data were further aggregated to 5-year monthly means and resampled to 0.01° spatial resolution to match the resolution of PA and NPA.

We used the MODIS ET and latent heat flux product (MOD16A2 version 6) (*61*) of 8-day temporal resolution and 500-m spatial resolution from 2014 to 2018 to quantify the latent heat difference between PAs and NPAs. MOD16A2 collection is derived on the basis of the logic of the Penman-Monteith equation by using daily meteorological reanalysis data with MODIS vegetation property dynamics, albedo, and land cover. We resampled MOD16A2 from 500-m to 0.01° spatial resolution to match the resolution of PA and NPA using bilinear interpolation.

The latent heat difference (ΔLE) and albedo difference ($\Delta Albedo$) between PAs and NPAs were calculated as

$$\Delta LE = LE_{\text{PA}} - LE_{\text{NPA}} \tag{3}$$

$$\Delta Albedo = Albedo_{\text{PA}} - Albedo_{\text{NPA}} \tag{4}$$

ΔLE values were calculated with MODIS ET and latent heat flux product (MOD16A2 V6). $\Delta Albedo$ was calculated from Eq. 3 with MODIS Bidirectional Reflectance Distribution Function and Albedo (BRDF/Albedo) dataset (MCD43A3 V6).

The net surface shortwave radiation difference (ΔSW) between PAs and NPAs in the same window was calculated as

$$\begin{aligned} \Delta SW &= (1 - Albedo_{\text{PA}}) \times SW_{\downarrow} - (1 - Albedo_{\text{NPA}}) \times SW_{\downarrow} \\ &= -\Delta Albedo \times SW_{\downarrow} \end{aligned} \tag{5}$$

where $SW_{\downarrow}$ is the downward shortwave radiation from Clouds and the Earth's Radiant Energy System Energy Balanced and Filled Surface products. Under clear-sky conditions, $SW_{\downarrow}$ is assumed to be homogeneously distributed in the 0.25° window.

The net surface longwave radiation difference (ΔLW) between PAs and NPAs in the same window was calculated as

$$\begin{aligned} \Delta LW &= (\varepsilon_{\text{PA}} - \varepsilon_{\text{NPA}}) \times LW_{\downarrow} - \\ &\quad \sigma(\varepsilon_{\text{PA}} \cdot LST_{\text{PA}}^4 - \varepsilon_{\text{NPA}} \cdot LST_{\text{NPA}}^4) \end{aligned} \tag{6}$$

where $(\varepsilon_{\text{PA}} - \varepsilon_{\text{NPA}}) \times LW_{\downarrow}$ is the downward longwave radiation difference between PA and NPA, which is negligible because the emissivity of PAs and NPAs (ε_{PA} and ε_{NPA}) is close for the same biome

and varies slightly across vegetated areas (*62*); $-\sigma (\varepsilon_{\text{PA}} \cdot LST_{\text{PA}}^4 - \varepsilon_{\text{NPA}} \cdot LST_{\text{NPA}}^4)$ is the upward longwave radiation difference between PAs and NPAs; and σ is the Stefan-Boltzmann constant ($5.67 \times 10^8 \, \text{Wm}^{-2} \, \text{K}^{-4}$).

We calculated the sensible heat (H) as the residue of the other energy components in Eq. 2. Therefore, the latent heat difference (ΔH) between PAs and NPAs in the same window was calculated with Eqs. 3, 5, and 6

$$\Delta H = H_{\text{PA}} - H_{\text{NPA}} = \Delta SH + \Delta LW - \Delta LE \tag{7}$$

We then presented $-(\Delta H + \Delta LE)$ to indicate the net effects of PAs compared to NPAs through evaporative cooling and turbulent heat loss.

Warming trend buffered by PAs

We calculated the fraction of protected biome in each 0.25° window. For each biome, the 0.25° windows were then classified according to their category of PA coverage as >10% (all the 0.25° windows with PA coverage greater than 10%), >20%, >30%, >40%, and >50%. This classification ensured that each 0.25° window included in the analysis had at least a 10% PA coverage, and an adequate number of windows were included to reduce the bias with overlaps of the windows for each category (table S3). The annual mean LST between 2003 and 2018 (16 years) was calculated for each biome and each category of PA coverage in each 0.25° window. The annual mean LST was also calculated for PAs only within the 0.25° windows for each biome and PA coverage category. The warming rate per decade (degrees Celsius per decade) of the 0.25° windows and PAs only within the 0.25° windows for each biome and each category of PA coverage was calculated as 10 times the slope of linear regression of the annual mean LST over 2003 to 2018 with the Theil-Sen estimator. We then calculated the mean warming rate of all the 0.25° windows per biome and per PA coverage category. We also evaluated the warming rate per decade of the 2-m air temperature using the European Centre for Medium-Range Weather Forecasts (ECMWF) ERA5 monthly reanalysis at 0.25° (*63*) for each biome and each category of PA coverage. The 2-m air temperatures, which are synthesized from standard weather stations outside natural or seminatural vegetation, indicate the macroclimate conditions (*29, 30*).

SUPPLEMENTARY MATERIALS

Supplementary material for this article is available at https://science.org/doi/10.1126/sciadv.abo0119

REFERENCES AND NOTES

1. K. S. Andam, P. J. Ferraro, A. Pfaff, G. A. Sanchez-Azofeifa, J. A. Robalino, Measuring the effectiveness of protected area networks in reducing deforestation. *Proc. Natl. Acad. Sci. U.S.A.* **105**, 16089–16094 (2008).
2. M. C. P. de Moraes, K. de Mello, R. H. Toppa, Protected areas and agricultural expansion: Biodiversity conservation versus economic growth in the Southeast of Brazil. *J. Environ. Manage.* **188**, 73–84 (2017).
3. L. Kehoe, A. Romero-Muñoz, E. Polaina, L. Estes, H. Kreft, T. Kuemmerle, Biodiversity at risk under future cropland expansion and intensification. *Nat. Ecol. Evol.* **1**, 1129–1135 (2017).
4. H. C. Flynn, L. M. i. Canals, E. Keller, H. King, S. Sim, A. Hastings, S. Wang, P. Smith, Quantifying global greenhouse gas emissions from land-use change for crop production. *Glob. Chang. Biol.* **18**, 1622–1635 (2012).
5. G. Duveiller, J. Hooker, A. Cescatti, The mark of vegetation change on Earth's surface energy balance. *Nat. Commun.* **9**, 679 (2018).
6. K. L. Findell, A. Berg, P. Gentine, J. P. Krasting, B. R. Lintner, S. Malyshev, J. A. Santanello Jr., E. Shevliakova, The impact of anthropogenic land use and land cover change on regional climate extremes. *Nat. Commun.* **8**, 989 (2017).

7. C. Román-Palacios, J. J. Wiens, Recent responses to climate change reveal the drivers of species extinction and survival. *Proc. Natl. Acad. Sci. U.S.A.* **117**, 4211–4217 (2020).

8. S. Govaert, P. Vangansbeke, H. Blondeel, K. Steppe, K. Verheyen, P. De Frenne, Rapid thermophilization of understorey plant communities in a 9 year-long temperate forest experiment. *J. Ecol.* **109**, 2434–2447 (2021).

9. J. R. Mawdsley, R. O'Malley, D. S. Ojima, A review of climate-change adaptation strategies for wildlife management and biodiversity conservation. *Conserv. Biol.* **23**, 1080–1089 (2009).

10. J. E. M. Watson, N. Dudley, D. B. Segan, M. Hockings, The performance and potential of protected areas. *Nature* **515**, 67–73 (2014).

11. P. R. Elsen, W. B. Monahan, E. R. Dougherty, A. M. Merenlender, Keeping pace with climate change in global terrestrial protected areas. *Sci. Adv.* **6**, eaay0814 (2020).

12. B. W. Griscom, J. Adams, P. W. Ellis, R. A. Houghton, G. Lomax, D. A. Miteva, W. H. Schlesinger, D. Shoch, J. V. Siikamäki, P. Smith, P. Woodbury, C. Zganjar, A. Blackman, J. Campari, R. T. Conant, C. Delgado, P. Elias, T. Gopalakrishna, M. R. Hamsik, M. Herrero, J. Kiesecker, E. Landis, L. Laestadius, S. M. Leavitt, S. Minnemeyer, S. Polasky, P. Potapov, F. E. Putz, J. Sanderman, M. Silvius, E. Wollenberg, J. Fargione, Natural climate solutions. *Proc. Natl. Acad. Sci.* **114**, 11645–11650 (2017).

13. R. Smith, Z. J. Cannizzo, E. Belle, L. Wenzel, Role of protected areas in climate change mitigation, adaptation, and disaster risk reduction, in *Climate Action. Encyclopedia of the UN Sustainable Development Goals*, W. Leal Filho, A. M. Azul, L. Brandli, P. G. Özuyar, T. Wall, Eds. (Springer, 2020), pp. 1–16.

14. E. Dinerstein, A. R. Joshi, C. Vynne, A. T. L. Lee, F. Pharand-Deschênes, M. França, S. Fernando, T. Birch, K. Burkart, G. P. Asner, D. Olson, A "Global Safety Net" to reverse biodiversity loss and stabilize Earth's climate. *Sci. Adv.* **6**, eabb2824 (2020).

15. J. M. Melillo, X. Lu, D. W. Kicklighter, J. M. Reilly, Y. Cai, A. P. Sokolov, Protected areas' role in climate-change mitigation. *Ambio* **45**, 133–145 (2016).

16. J. Winckler, Q. Lejeune, C. H. Reick, J. Pongratz, Nonlocal effects dominate the global mean surface temperature response to the biogeophysical effects of deforestation. *Geophys. Res. Lett.* **46**, 745–755 (2019).

17. N. Devaraju, N. de Noblet-Ducoudré, B. Quesada, G. Bala, Quantifying the relative importance of direct and indirect biophysical effects of deforestation on surface temperature and teleconnections. *J. Climate* **31**, 3811–3829 (2018).

18. D. Scherrer, C. Körner, Infra-red thermometry of alpine landscapes challenges climatic warming projections. *Glob. Chang. Biol.* **16**, 2602–2613 (2010).

19. P. De Frenne, F. Rodriguez-Sánchez, D. A. Coomes, L. Baeten, G. Verstraeten, M. Vellend, M. Bernhardt-Romermann, C. D. Brown, J. Brunet, J. Cornelis, G. M. Decocq, H. Dierschke, O. Eriksson, F. S. Gilliam, R. Hédl, T. Heinken, M. Hermy, P. Hommel, M. A. Jenkins, D. L. Kelly, K. J. Kirby, F. J. G. Mitchell, T. Naaf, M. Newman, G. Peterken, P. Petřík, J. Schultz, G. Sonnier, H. Van Calster, D. M. Waller, G.-R. Walther, P. S. White, K. D. Woods, M. Wulf, B. J. Graae, K. Verheyen, Microclimate moderates plant responses to macroclimate warming. *Proc. Natl. Acad. Sci.* **110**, 18561–18565 (2013).

20. F. Zellweger, P. de Frenne, J. Lenoir, P. Vangansbeke, K. Verheyen, M. Bernhardt-Römermann, L. Baeten, R. Hédl, I. Berki, J. Brunet, H. van Calster, M. Chudomelová, G. Decocq, T. Dirnböck, T. Durak, T. Heinken, B. Jaroszewicz, M. Kopecký, F. Máliš, M. Macek, M. Malicki, T. Naaf, T. A. Nagel, A. Ortmann-Ajkai, P. Petřík, R. Pielech, K. Reczyńska, W. Schmidt, T. Standovár, K. Świerkosz, B. Teleki, O. Vild, M. Wulf, D. Coomes, Forest microclimate dynamics drive plant responses to warming. *Science* **368**, 772–775 (2020).

21. Y. Li, M. Zhao, S. Motesharrei, Q. Mu, E. Kalnay, S. Li, Local cooling and warming effects of forests based on Satellite Observations. *Nat. Commun.* **6**, 6603 (2015).

22. R. Alkama, A. Cescatti, Climate change: Biophysical climate impacts of recent changes in global forest cover. *Science* **351**, 600–604 (2016).

23. A. J. Rigden, D. Li, Attribution of surface temperature anomalies induced by land use and land cover changes. *Geophys. Res. Lett.* **44**, 6814–6822 (2017).

24. X. Lee, M. L. Goulden, D. Y. Hollinger, A. Barr, T. A. Black, G. Bohrer, R. Bracho, B. Drake, A. Goldstein, L. Gu, G. Katul, T. Kolb, B. E. Law, H. Margolis, T. Meyers, R. Monson, W. Munger, R. Oren, K. T. P. U, A. D. Richardson, H. P. Schmid, R. Staebler, S. Wofsy, L. Zhao, Observed increase in local cooling effect of deforestation at higher latitudes. *Nature* **479**, 384–387 (2011).

25. UNEP-WCMC, IUCN, "Protected Planet: The World Database on Protected Areas (WDPA), October 2018, Cambridge, UK: UNEP-WCMC and IUCN" (UNEP-WCMC and IUCN, 2018); www.protectedplanet.net.

26. M. Friedl, D. Sulla-Menashe, "MCD12Q1 MODIS/Terra+Aqua Land Cover Type Yearly L3 Global 500m SIN Grid V006" (NASA EOSDIS Land Processes DAAC, 2019).

27. C. L. Gray, S. L. L. Hill, T. Newbold, L. N. Hudson, L. Börger, S. Contu, A. J. Hoskins, S. Ferrier, A. Purvis, J. P. W. Scharlemann, Local biodiversity is higher inside than outside terrestrial protected areas worldwide. *Nat. Commun.* **7**, 12306 (2016).

28. Z. Wan, S. Hook, G. Hulley, "MYD11C2 MODIS/Aqua Land Surface Temperature/Emissivity 8-Day L3 Global 0.05Deg CMG V006. (NASA EOSDIS Land Processes DAAC, 2015); https://doi.org/10.5067/MODIS/MYD11C2.006.

29. P. De Frenne, F. Zellweger, F. Rodríguez-Sánchez, B. R. Scheffers, K. Hylander, M. Luoto, M. Vellend, K. Verheyen, J. Lenoir, Global buffering of temperatures under forest canopies. *Nat. Ecol. Evol.* **3**, 744–749 (2019).

30. P. De Frenne, K. Verheyen, Weather stations lack forest data. *Science* **351**, 234 (2016).

31. Y.-K. Lim, M. Cai, E. Kalnay, L. Zhou, Impact of vegetation types on surface temperature change. *J. Appl. Meteorol. Climatol.* **47**, 411–424 (2008).

32. D. J. Mildrexler, M. Zhao, S. W. Running, A global comparison between station air temperatures and MODIS land surface temperatures reveals the cooling role of forests. *J. Geophys. Res. Biogeo.* **116**, G03025 (2011).

33. J. M. Bennett, J. Sunday, P. Calosi, F. Villalobos, B. Martínez, R. Molina-Venegas, M. B. Araújo, A. C. Algar, S. Clusella-Trullas, B. A. Hawkins, S. A. Keith, I. Kühn, C. Rahbek, L. Rodríguez, A. Singer, I. Morales-Castilla, M. Á. Olalla-Tárraga, The evolution of critical thermal limits of life on Earth. *Nat. Commun.* **12**, 1198 (2021).

34. M. C. Urban, Accelerating extinction risk from climate change. *Science* **348**, 571–573 (2015).

35. J. Alroy, Effects of habitat disturbance on tropical forest biodiversity. *Proc. Natl. Acad. Sci. U.S.A.* **114**, 6056–6061 (2017).

36. J. M. Sunday, A. E. Bates, M. R. Kearney, R. K. Colwell, N. K. Dulvy, J. T. Longino, R. B. Huey, Thermal-safety margins and the necessity of thermoregulatory behavior across latitude and elevation. *Proc. Natl. Acad. Sci. U.S.A.* **111**, 5610–5615 (2014).

37. J. J. Tewksbury, R. B. Huey, C. A. Deutsch, Ecology: Putting the heat on tropical animals. *Science* **320**, 1296–1297 (2008).

38. M. E. Dillon, G. Wang, R. B. Huey, Global metabolic impacts of recent climate warming. *Nature* **467**, 704–706 (2010).

39. P. Smith, S. J. Davis, F. Creutzig, S. Fuss, J. Minx, B. Gabrielle, E. Kato, R. B. Jackson, A. Cowie, E. Kriegler, D. P. van Vuuren, J. Rogelj, P. Ciais, J. Milne, J. G. Canadell, D. M. Collum, G. Peters, R. Andrew, V. Krey, G. Shrestha, P. Friedlingstein, T. Gasser, A. Grübler, W. K. Heidug, M. Jonas, C. D. Jones, F. Kraxner, E. Littleton, J. Lowe, J. R. Moreira, N. Nakicenovic, M. Obersteiner, A. Patwardhan, M. Rogner, E. Rubin, A. Sharifi, A. Torvanger, Y. Yamagata, J. Edmonds, C. Yongsung, Biophysical and economic limits to negative CO_2 emissions. *Nat. Clim. Chang.* **6**, 42–50 (2016).

40. J. Sunday, J. M. Bennett, P. Calosi, S. Clusella-Trullas, S. Gravel, A. L. Hargreaves, F. P. Leiva, W. C. E. P. Verberk, M. Á. Olalla-Tárraga, I. Morales-Castilla, Thermal tolerance patterns across latitude and elevation. *Phil. Trans. R. Soc. B.* **374**, 20190036 (2019).

41. L. T. Lancaster, A. M. Humphreys, Global variation in the thermal tolerances of plants. *Proc. Natl. Acad. Sci. U.S.A.* **117**, 13580–13587 (2020).

42. F. S. Gilliam, Forest ecosystems of temperate climatic regions: From ancient use to climate change. *New Phytol.* **212**, 871–887 (2016).

43. J. L. McGuire, J. J. Lawler, B. H. McRae, T. A. Nuñez, D. M. Theobald, Achieving climate connectivity in a fragmented landscape. *Proc. Natl. Acad. Sci. U.S.A.* **113**, 7195–7200 (2016).

44. S. A. Parks, C. Carroll, S. Z. Dobrowski, B. W. Allred, Human land uses reduce climate connectivity across North America. *Glob. Chang. Biol.* **26**, 2944–2955 (2020).

45. T. L. Morelli, C. W. Barrows, A. R. Ramirez, J. M. Cartwright, D. D. Ackerly, T. D. Eaves, J. L. Ebersole, M. A. Krawchuk, B. H. Letcher, M. F. Mahalovich, G. W. Meigs, J. L. Michalak, C. I. Millar, R. M. Quiñones, D. Stralberg, J. H. Thorne, Climate-change refugia: Biodiversity in the slow lane. *Front. Ecol. Environ.* **18**, 228–234 (2020).

46. J. Jin, N. L. Miller, Regional simulations to quantify land use change and irrigation impacts on hydroclimate in the California Central Valley. *Theor. Appl. Climatol.* **104**, 429–442 (2011).

47. J. Kala, M. Decker, J. F. Exbrayat, A. J. Pitman, C. Carouge, J. P. Evans, G. Abramowitz, D. Mocko, Influence of leaf area index prescriptions on simulations of heat, moisture, and carbon fluxes. *J. Hydrometeorol.* **15**, 489–503 (2014).

48. C. Chen, D. Li, Y. Li, S. Piao, X. Wang, M. Huang, P. Gentine, R. R. Nemani, R. B. Myneni, Biophysical impacts of Earth greening largely controlled by aerodynamic resistance. *Sci. Adv.* **6**, eabb1981 (2020).

49. M. M. Loranty, L. T. Berner, S. J. Goetz, Y. Jin, J. T. Randerson, Vegetation controls on northern high latitude snow-albedo feedback: Observations and CMIP5 model simulations. *Glob. Chang. Biol.* **20**, 594–606 (2014).

50. P. G. Curtis, C. M. Slay, N. L. Harris, A. Tyukavina, M. C. Hansen, Classifying drivers of global forest loss. *Science* **361**, 1108–1111 (2018).

51. K. A. Poiani, B. D. Richter, M. G. Anderson, H. E. Richter, Biodiversity conservation at multiple scales: Functional sites, landscapes, and networks. *Bioscience* **50**, 133–146 (2000).

52. T. Jucker, S. R. Hardwick, S. Both, D. M. O. Elias, R. M. Ewers, D. T. Milodowski, T. Swinfield, D. A. Coomes, Canopy structure and topography jointly constrain the microclimate of human-modified tropical landscapes. *Glob. Chang. Biol.* **24**, 5243–5258 (2018).

53. D. Scherrer, C. Körner, Topographically controlled thermal-habitat differentiation buffers alpine plant diversity against climate warming. *J. Biogeogr.* **38**, 406–416 (2011).

54. H. Ohashi, T. Hasegawa, A. Hirata, S. Fujimori, K. Takahashi, I. Tsuyama, K. Nakao, Y. Kominami, N. Tanaka, Y. Hijioka, T. Matsui, Biodiversity can benefit from climate stabilization despite adverse side effects of land-based mitigation. *Nat. Commun.* **10**, 5240 (2019).

55. D. T. Sandwell, W. H. F. Smith, J. J. Becker, "SRTM30+ Global 1-km Digital Elevation Model (DEM): Version 11: Land Surface" (2014); http://pacioos.org/metadata/srtm30plus_v11_land.html.

56. T. Myneni, R., Knyazikhin, Y., Park, "MOD15A2H MODIS/Terra Leaf Area Index/FPAR 8-Day L4 Global 500m SIN Grid V006" (NASA EOSDIS Land Processes DAAC, 2015); https://doi.org/10.5067/MODIS/MOD15A2H.006.

57. J. Geldmann, A. Manica, N. D. Burgess, L. Coad, A. Balmford, A global-level assessment of the effectiveness of protected areas at resisting anthropogenic pressures. *Proc. Natl. Acad. Sci. U.S.A.* **116**, 23209–23215 (2019).

58. M. Cook, J. R. Schott, J. Mandel, N. Raqueno, Development of an operational calibration methodology for the Landsat thermal data archive and initial testing of the atmospheric compensation component of a land surface temperature (LST) product from the archive. *Remote Sens. (Basel)* **6**, 11244–11266 (2014).

59. M. Jin, R. E. Dickinson, Land surface skin temperature climatology: Benefitting from the strengths of satellite observations. *Environ. Res. Lett.* **5**, 44004 (2010).

60. C. Schaaf, Z. Wang, "MCD43C3 MODIS/Terra+Aqua BRDF/Albedo Albedo Daily L3 Global 0.05Deg CMG V006" (NASA LP DAAC, 2015); http://doi.org/10.5067/MODIS/MCD43C3.006.

61. S. Running, Q. Mu, M. Zhao, "MOD16A2 MODIS/Terra Net Evapotranspiration 8-Day L4 Global 500m SIN Grid V006" (NASA LP DAAC, 2017); http://doi.org/10.5067/MODIS/MOD16A2.006.

62. M. Jin, S. Liang, An improved land surface emissivity parameter for land surface models using global remote sensing observations. *J. Climate* **19**, 2867–2881 (2006).

63. H. Hersbach, B. Bell, P. Berrisford, S. Hirahara, A. Horányi, J. Muñoz-Sabater, J. Nicolas, C. Peubey, R. Radu, D. Schepers, A. Simmons, C. Soci, S. Abdalla, X. Abellan, G. Balsamo, P. Bechtold, G. Biavati, J. Bidlot, M. Bonavita, G. De Chiara, P. Dahlgren, D. Dee, M. Diamantakis, R. Dragani, J. Flemming, R. Forbes, M. Fuentes, A. Geer, L. Haimberger, S. Healy, R. J. Hogan, E. Hólm, M. Janisková, S. Keeley, P. Laloyaux, P. Lopez, C. Lupu, G. Radnoti, P. de Rosnay, I. Rozum, F. Vamborg, S. Villaume, J.-N. Thépaut, The ERA5 global reanalysis. *Q. J. Roy. Meteorol. Soc.* **146**, 1999–2049 (2020).